Hindawi
Advances in Civil Engineering
Volume 2020, Article ID 4536365, 13 pages
https://doi.org/10.1155/2020/4536365

Research Article

Reaction Spectrum Comparative Analysis of Seismic Performance of 62 m CFST Bridge with Curved-String Truss before and after Reinforcement

Daihai Chen,[1] Yinxin Li,[1] Zheng Li,[1] Yilin Fang,[2] Laijing Ma,[1] and Fengrui Ma[1]

[1]*Institute of Bridge Engineering, School of Civil Engineering, Zhengzhou University, Zhengzhou 450001, China*
[2]*Henan Expressway Development Co., Ltd, Zhengzhou 450052, China*

Correspondence should be addressed to Zheng Li; lizhengcdh@zzu.edu.cn

Received 23 September 2019; Revised 21 February 2020; Accepted 11 June 2020; Published 14 July 2020

Academic Editor: Mostafa Sharifzadeh

Taking a 62 m CFST bridge with a curved-string truss as the research object, according to its reinforcement scheme, the spatial finite element models of the bridge before and after reinforcement were established by using the general finite element software ANSYS. The natural frequencies of the bridge before and after reinforcement were calculated, and the seismic performance of the bridge was analyzed by using the response spectrum method. The results show that the frequencies of the reinforced bridges increase in varying degrees, especially the vertical and torsional frequencies. Before and after reinforcement, the maximum axial force in the upper chord of the bridge is the largest, and the shear force and bending moment are small. The maximum internal force appears at the two ends of the upper chord. This position should be regarded as the weak link of the bridge seismic resistance. Under the same conditions, the axial force of the bridge after reinforcement is reduced by about 30% compared with that before reinforcement, and the displacement of the bridge after reinforcement is reduced in varying degrees. The reinforcement measures can improve the lateral and vertical stiffness of the bridge, especially the stiffness of the deck system.

1. Introduction

The CFST bridge with curved-string truss has the characteristics of flexible and diverse component layout, beautiful appearance, strong bearing capacity, and large span capacity, which has been applied in urban bridge engineering. The structure of this type of bridge is different from that of a CFST arch bridge, and their mechanical characteristics, especially their seismic performance, are also different.

At present, many scholars have done much work on the seismic performance of CFST bridges. Sevim et al. [1] investigated the effects of near and far fault ground motion on the seismic behavior of historical arch bridges through a combined numerical and experimental evaluation. Results indicated that near-fault ground motion imposes higher seismic demand on the arch bridge observed in both higher displacements and stresses. In the paper by Farahani and Maalek [2], through a detailed three-dimensional finite element modeling and analysis of an actual existing deck-type RC arch bridge, some useful quantitative information has been derived that may serve for a better understanding of the seismic behavior of such arch bridges. Zampieri et al. [3, 4] established a kinematic analysis method for the lateral seismic capacity of multi-span slender pier masonry bridges. It could be used for the preliminary evaluation of earthquakes and take the form of a useful tool for identifying the best retrofit strategies for each masonry bridge structure in the function of its geometrical characteristics. Shao et al. [5] evaluated the seismic behavior of the members by quantifying the bending moment and plastic rotation requirements and capabilities of the flexible members and determined the seismic applicability of a long-span railway concrete upper-deck arch bridge with CFST rigid skeleton rib. Porto et al. [6] evaluated the seismic performance of single-span and multi-span masonry arch bridges through limit state analysis and priority seismic reconstruction measures and comprehensively studied the seismic performance of reinforced concrete arch bridges. Deng et al. [7] used ABAQUS software to

model the reference reinforced concrete arch bridges and determined the longitudinal and lateral seismic performance under different seismic intensities. Li et al. [8] took a half-through steel truss arch bridge as an example. A seismic analysis was conducted with a nonlinear finite element method. The influence of seismic wave direction and wave-passage on seismic behaviors was analyzed as well as the superstructure and arch ring interaction which was mostly related to the supported bearings and wind-resistant springs. Xiao et al. [9] suggested that, in the construction of arch bridges with karst cave foundation, the seismic design should be strengthened for key parts such as arch ribs and chords to reduce the damage of arch bridges caused by the earthquake. Yangjing et al. [10] studied the influence of structural design parameters on the seismic performance and applicability of CFST lattice high pier continuous girder bridges. Huang et al. [11] explored the seismic behaviors of CFST arch bridges, by establishing a scaled 1 : 10 model of CFST arch rib with fully compensative mass. The results show the transverse seismic response is more distinct than that longitudinal response, and the bidirectional excitation has much larger responses than the single excitation. Han et al. [12] reported a series of bending tests on CFST trusses and hybrid CFST trusses. Hollow tubular trusses were also tested for comparison. The results showed that both the infill concrete and concrete slab improved the flexural performance of the truss notably. Bo et al. [13] found that the longitudinal stiffness of the deck long-span arch bridge was far greater than the lateral stiffness, and the arch ribs were resistant to the earthquake. The most dangerous section in seismic design was the arch foot section, with the largest internal force in seismic response. Shixiong et al. [14] found that the internal force in seismic response of the middle section of the main arch rib was smaller, while the internal force in seismic response of the arch foot section and L/4~3 L/8 section was relatively larger. Álvarez et al. [15] analyzed the influence of the change of axial force on the ductility and strength of long-span bridge in the earthquake time history analysis, the expected ductility requirements of arch shape, and the spatial variability of earthquake response. Through analysis, Xiaobing and Yijuan [16] put forward measures such as increasing the transverse brace stiffness and wrapping the arch foot in concrete to enhance the seismic performance of tied-arch bridge. Zhiming et al. [17] found that the traveling wave effect increased the internal force of arch bridges to varying degrees, and the increase of the axial force at the arch foot was greater than that of the bending moment, and there was no direct relationship between the increase of the axial force and the peak acceleration.

Yan and Shide [18] studied and discussed the seismic performance of the CFST arch bridge from the perspective of Liapunov motion stability and put forward a new evaluation method. Wang et al. [19] analyzed the nonuniform seismic response of the CFST arch bridge, and the results showed that the effect of local site effect was greater than that of traveling wave effect and partial coherence effect. Yuan et al. [20] investigated the behavior of PCFST bridge piers under bidirectional seismic excitations. The result shows deformation capacity deteriorated considerably when subjected to bidirectional dynamic loadings, and the seismic behavior of PCFST bridge piers can be effectively improved if the concrete fill height is significantly increased. Yang et al. [21, 22] investigated the seismic behavior of four-legged square CFST latticed members. The experimental results clarify that the four-legged square CFST latticed specimens outperform the reference hollow steel ones in terms of hysteretic behavior. But for the CFST latticed specimens, outward tube buckling at the bottom of the chords combined with cracking at the front K-shaped chord-brace connections are found to be the main failure patterns. Xiaozhen et al. [23] comprehensively studied that the spatial variability effect of the seismic wave will have a significant impact on the seismic response of continuous beam arch bridge, and only considering the uniform seismic excitation may overestimate the seismic response of the bridge structure. Yadav et al. [24] studied the hysteretic behavior of CFST columns under cyclic loading. And experimental results show failure of CFST laced column is ductile; the cracks initiate from RC-web and the column fails due to the formation of plastic hinge at bottom of CFST limbs. Lateral load carrying capacity increases with the increase in the diameter of steel tubes and the thickness of RC-web. Ductility increases with increase in the diameter of steel tubes and decreases with increase in the thickness of RC-web. Di et al. [25] found that the dynamic failure of the long-span CFST arch bridge under a strong earthquake is the result of the joint action of structural displacement and plastic development. Jianxin et al. [26] put forward the strengthening scheme of strengthening the bottom chord and the upper and lower horizontal and longitudinal diagonal members for five single line steel trusses with different spans and insufficient transverse direction. After strengthening, the natural vibration frequency of the trusses is increased, and the transverse amplitude in the middle of the span is greatly reduced. Chen et al. [27] developed an advanced nonlinear analysis formwork that can account for the material interaction and confinement in CFST trusses with the reliability analysis of CFST truss with random imperfections. Kai et al. [28] studied that the steel arch strengthened by a prestressed broken line hinged steel arch can effectively share and improve the self-weight internal force of the arch rib and significantly improve its compressive capacity. Ma et al. [29] presented an experimental investigation of the seismic performance of joints of concrete-encased concrete-filled steel tubular (CFST) column. Four types of typical failure modes are found, and the seismic performance of the composite joint is also evaluated by several indexes, such as rigidity degradation, strength degradation, ductility, and energy dissipation.

According to the statistics of literature [30], more than 50% of the existing CFST arch bridges in China after the millennium have a span of more than 100 meters, which belongs to long-span bridges. However, as a rare type of bridge, there is relatively little research on the seismic performance of concrete-filled steel tubular curved truss bridges. Therefore, this paper takes a concrete-filled steel tubular curved truss bridge as the research object. According

to its reinforcement scheme, the spatial finite element model before and after reinforcement is established by ANSYS. The response spectrum method is used to compare and analyze its seismic response and evaluate the improvement effect of strengthening measures on its seismic performance. It provides a reference for seismic design and reinforcement and maintenance of this type of bridge.

2. Finite Element Models of the Bridge

2.1. General Description of the Bridge

2.1.1. Bridge before Reinforcement. A through CFST bridge with curved string truss is supported system. The span of the bridge is 62 m, and the width is 28.8 m. The main truss spacing is 16.4 m, and the maximum height of the truss beam is 12.066 m. The upper chord is a CFST structure with a diameter of 0.9 m. The steel tube is filled with C40 concrete, and the wall thickness of the steel tube is 16 mm. The lower chord is an open steel box girder. The height of the steel box girder is 0.64 m, the top width of the steel box girder is 0.8 m, and the bottom width of the steel box girder is 0.56 m. Three types of hollow steel tubes are used for web rod and cross brace. These three kinds of hollow steel tubes are $\Phi 600 \times 8$ mm, $\Phi 600 \times 12$ mm, and $\Phi 600 \times 16$ mm, respectively. The spacing of beams is 5 m, and the thickness of the deck is 5 cm.

(1) Main Truss. The main cross section dimensions of the main truss are shown in Figures 1–4.

(2) Steel Crossbeam. The section of the open steel box girder is shown in Figure 5.

(3) Tie Beam. The two tied girders are 16.4 m apart along the bridge transversely. Open-ended steel box girders are adopted, and their cross-sections are shown in Figure 6.

2.1.2. Bridge after Reinforcement. After more than 20 years of service, the vertical vibration of the bridge has been aggravated. According to the reinforcement scheme, it needs to be strengthened and maintained. The overall stability of the bridge structure is improved by strengthening the end of the top chord, adding suspenders and truss beams to the oblique web, increasing the height of the bridge crossbeam, tied beam web, and deck system, adding two small crossbeams in the joints, and applying U-shaped rib orthotropic plate [31] in the steel bridge deck.

(1) Reinforcement of the End of the Upper Chord. Firstly, the upper chord is polished within the reinforcement range of the end of the upper chord. Then, the shear nails are welded on the surface of the upper chord. Twelve sheer nails are evenly arranged on each section perpendicular to the axis of the upper chord. The spacing of the section along the axis of the upper chord is 30 cm. The sizes of reinforced concrete and steel sheath of the upper chord are shown in Figure 7.

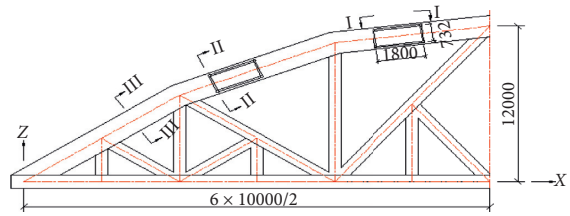

Figure 1: Elevation of 1/2 of the main truss (unit: mm).

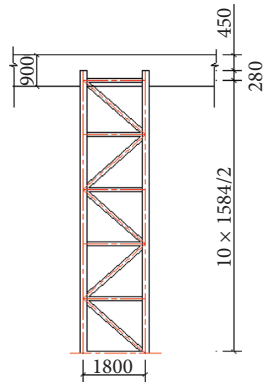

Figure 2: I-I section (unit: mm).

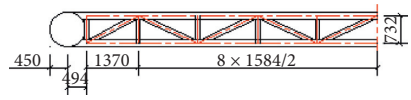

Figure 3: II-II section (unit: mm).

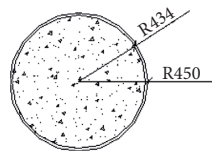

Figure 4: III-III section (unit: mm).

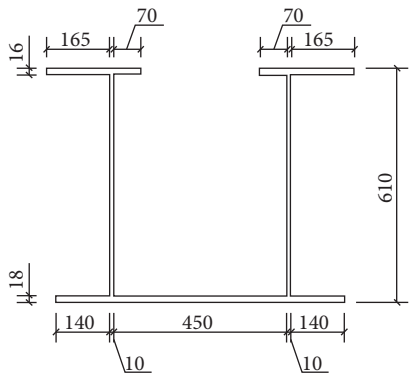

Figure 5: Diagram of a cross section of the steel crossbeam (unit: mm).

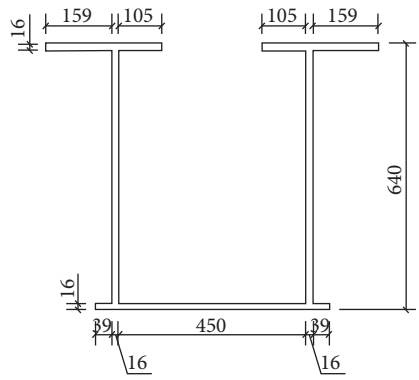

Figure 6: Section diagram of the tied beam (unit: mm).

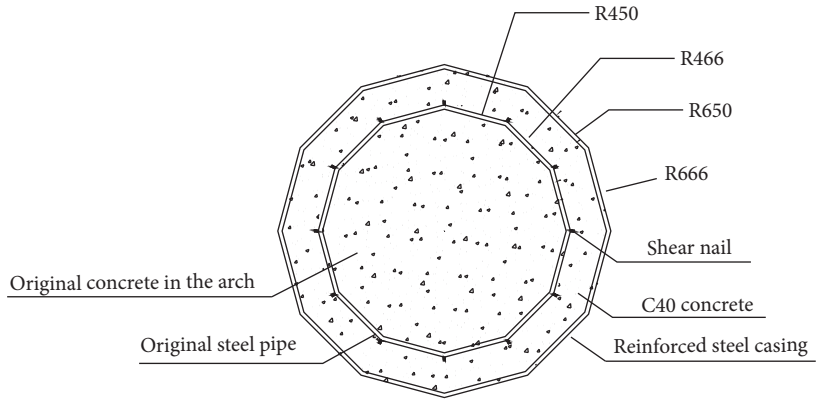

Figure 7: Diagram of the reinforcement section (unit: mm).

(2) Reinforcement of Web

(1) Adding Hangers

Setting two groups of flexible suspenders beside each vertical web member can reduce the occurrence of a larger stress amplitude of the web member. At the same time, in the fatigue failure period of the joint, the original vertical web member is replaced by the original vertical web member to bear the vertical force. The original design web bears high tensile stress, so the initial stress is applied to the rear suspender to share the load of the original web and improve the web force. In order not to affect the mechanical performance of the original bridge and not to destroy the integrity of the original bridge, the joints on the new suspenders are arranged by the riding span. The special joint design of the upper chord of the suspender's span position ensures that it meets the requirement of bearing the radial pressure of the suspender. The lower joints are designed with steel box girders, which are used as anchorage points for suspenders. The steel box is welded on the webs of the elevated cross girders. In this way, the load acting on the beam can be directly borne by the suspender, and the force is clear.

(2) Reinforcement of Inclined Web

Given the large fatigue stress amplitude of the oblique webs of truss beams, the reinforcement method of oblique webs and truss beams is considered. The reinforcement scheme is shown in Figure 8.

(3) Reinforcement of Bridge Deck System. The orthotropic plate with a U-shaped rib is used in the steel bridge deck. Compared with the open rib, the U-shaped rib has the advantages of saving material and good overall stability. The schematic diagram of the integral steel deck system is shown in Figures 9 and 10.

(1) Reinforcement of Crossbeam

In order to improve the transverse rigidity of the bridge, the web height of the beam is increased on the basis of the original beam. The cross section after strengthening is shown in Figure 11.

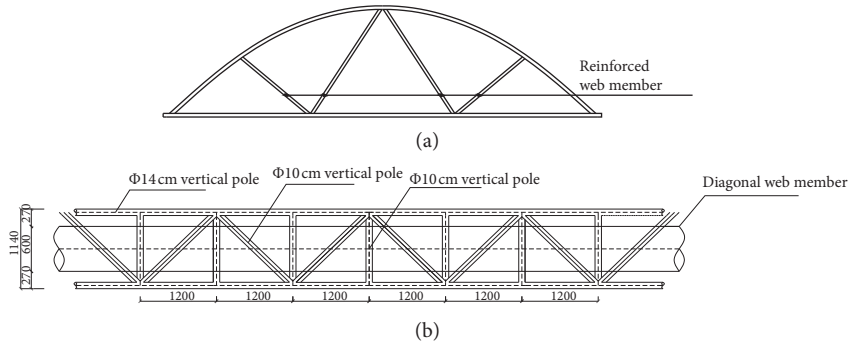

Figure 8: (a) Diagram of reinforcement location of webs. (b) Drawing of web reinforcement truss structure (unit: mm).

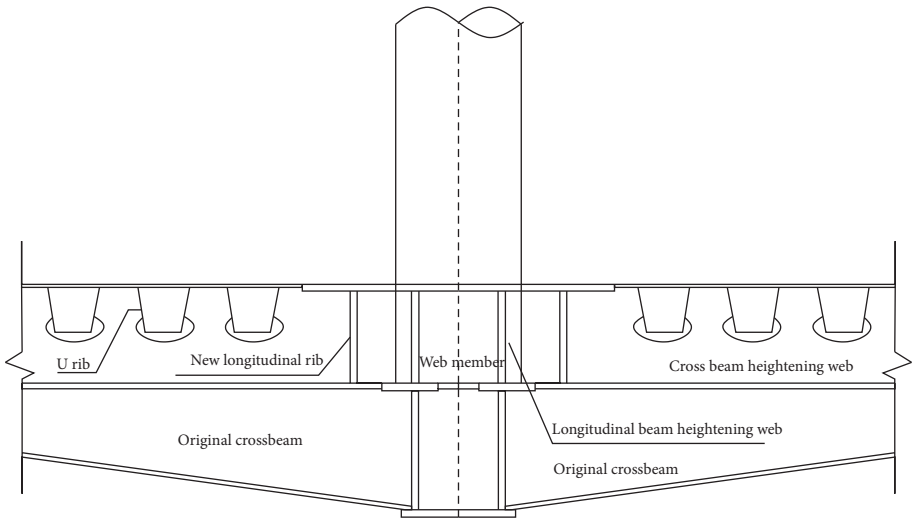

Figure 9: Section diagram of the integral steel deck system.

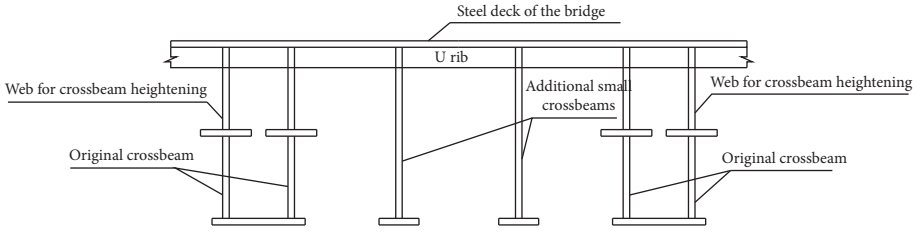

Figure 10: Elevation of the integral steel deck system.

(2) Reinforcement of Longitudinal Beam (Tie Beam)

In order to improve the longitudinal stiffness of the bridge, the web height of the longitudinal beam is increased based on the original longitudinal beam. The section of the reinforced longitudinal beam is shown in Figure 12.

(3) Adding Small Crossbeams

The spacing of the crossbeams of the original bridge is 5 m. Two small crossbeams are added to each section of the crossbeams to support the force. The section with additional small crossbeams is shown in Figure 13.

2.2. Establishment of a Finite Element Model of the Bridge. The finite element models of the bridge before and after reinforcement were built using the finite element software ANSYS®. The double-element method [32] was used to simulate the CFST structure of the upper chord. The steel tube and the concrete elements were included in the model and simulated by common nodes mode. The upper chord

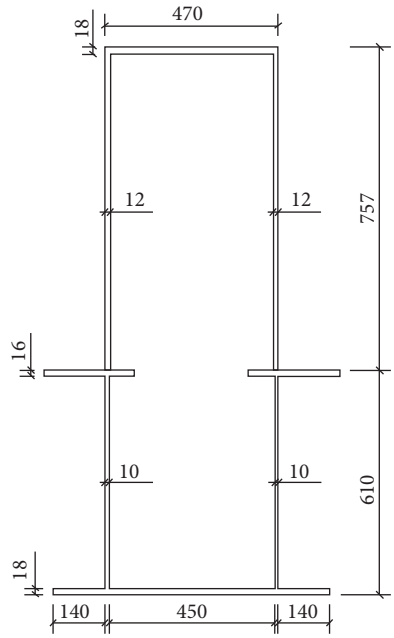

Figure 11: Diagram of strengthened cross section (unit: mm).

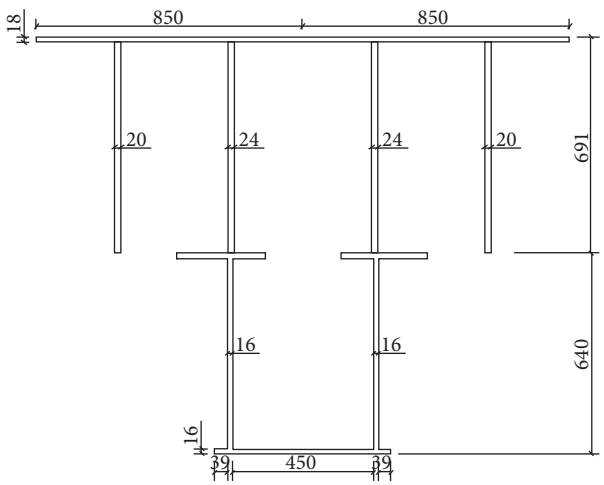

Figure 12: Section diagram of the reinforced longitudinal beam (unit: mm).

and the web member were simulated by using beam189 elements; the lower chord, the crossbeam, and the cross brace were discretized by using beam188 elements; and the prestressed steel strand was simulated by using the 3-dimensional rod element, i.e., Link 8 element; the concrete bridge deck was discretized by using Shell63 element. The cross bracing and the main winding are realized by establishing the master-slave node constraint to realize the degree of freedom coupling between the nodes. The above chord node is the master node, and the traverse end node is the slave node. According to the actual situation of the bridge, the left side of the upper string is fixed hinge support, and the other side is a horizontal one-way movable support. The right side of the upper string is a longitudinal one-way movable support, and the other side is two-way sliding hinge

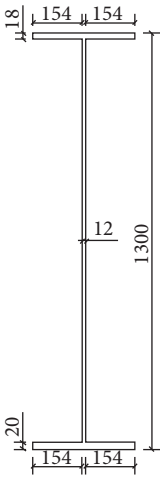

Figure 13: Diagram of a cross section of the small beam (unit: mm).

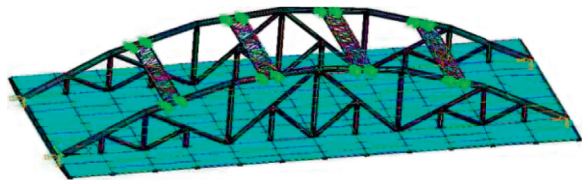

Figure 14: Finite element model of the bridge before reinforcement.

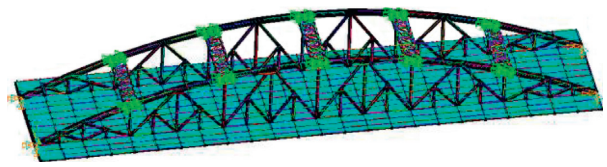

Figure 15: Finite element model of the reinforced bridge.

support. Before reinforcement, the bridge had 621 nodes and 1166 elements, which included 978 beam elements and 188 plate elements, as shown in Figure 14.

The U rib is converted to the deck thickness by the moment of inertia of the section and is used as a simulation of the bridge steel deck after reinforcement. The truss beam reinforced truss beam is converted into an equivalent rectangular section by the line stiffness equivalent principle. The added boom is simulated with a Link8 element, taking into account the initial tension of the boom in the form of initial strain. After reinforcement, the bridge has a total of 1115 nodes and 2306 elements, which included 1662 beam elements and 644 plate elements, as shown in Figure 15.

3. Analysis of Natural Vibration Characteristics

To analyze the natural vibration characteristics of the bridge, the Lanczos method in ANSYS modal analysis was used to calculate the natural vibration frequencies of the bridge before and after the reinforcement. Tables 1 and 2 list the characteristics of the first 10 frequencies and modes of the

Table 1: The first 10-order natural vibration characteristics of the bridge before reinforcement.

Modal number	Frequency (Hz)	Cycle (s)	Mode shape characteristics
1	1.741	0.574	Transverse first-order vibration of the main truss
2	2.982	0.335	Vertical vibration of the bridge deck
3	3.329	0.300	Torsional vibration of bridge deck
4	3.335	0.300	Transverse second-order vibration of main truss
5	3.487	0.287	Vertical vibration of the bridge deck
6	3.492	0.286	Full bridge torsion of the first-order vibration, vertical vibration of the bridge deck
7	3.808	0.263	Vertical vibration of the bridge deck
8	4.123	0.243	Full bridge torsion second-order vibration, vertical vibration of the bridge deck
9	4.216	0.237	Vertical first-order vibration of the whole bridge
10	4.408	0.227	Vertical vibration of the bridge deck

Table 2: The first 10-order natural vibration characteristics of the bridge after reinforcement.

Modal number	Frequency (Hz)	Cycle (s)	Mode shape characteristics
1	2.103	0.476	Transverse first-order vibration of the main truss
2	4.010	0.249	Transverse second-order vibration of main truss
3	5.164	0.194	Vertical first-order vibration of the whole bridge
4	5.741	0.174	Full bridge torsion of the first-order vibration, vertical vibration of the bridge deck
5	5.935	0.168	Transverse third-order vibration of the main truss
6	6.433	0.155	Vertical second-order vibration of the whole bridge
7	6.816	0.147	Full bridge torsion second-order vibration, vertical vibration of the bridge deck
8	8.464	0.118	Transverse fourth-order vibration of the main truss
9	8.628	0.116	Vertical third-order vibration of the whole bridge
10	9.078	0.110	Full bridge torsion third-order vibration, vertical vibration of the bridge deck

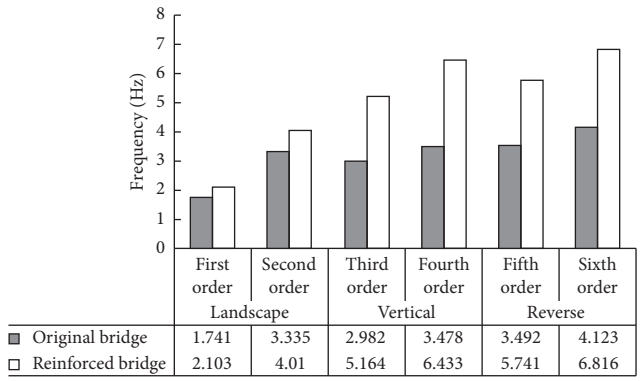

Figure 16: Comparison of the natural vibration frequencies of the bridge before and after reinforcement.

bridge. The comparison of the natural vibration characteristics of the bridge is shown in Figure 16.

Vibration modes of such bridges are complicated in Tables 1 and 2. The main vibration modes include lateral vibration of the main raft, vertical vibration of the bridge deck, vertical vibration, and torsional vibration of the bridge. The first mode of vibration before and after reinforcement is transverse vibration outside the plane of the main truss. Torsional vibration of bridges occurs after transverse and vertical vibration.

It shows that the transverse stiffness of the main truss of this type of bridge is relatively weak, and the torsional stiffness is substantially higher than its transverse and vertical stiffness. The second-order vibration mode of the bridge before reinforcement is the vertical vibration of the bridge deck. After reinforcement, it becomes the primary lateral vibration. After increasing the height of the longitudinal beam of the plateau bridge, adding small beams, and rebuilding the bridge deck, the bridge deck stiffness is significantly improved. Figure 16 shows the frequencies of the bridge after reinforcement has increased to varying degrees; in particular, the vertical and torsional frequencies of the bridges increase significantly.

4. Seismic Response Spectrum Analysis of the Bridge before and after Reinforcement

The seismic response of the concrete-filled steel tubular curved truss girder bridge before and after reinforcement was analyzed by using ANSYS, based on the finite element

model. The area where the project is located belongs to the category II site, which is a 7-degree seismic fortification area.

The horizontal acceleration response spectrum with the corresponding damping ratio of 0.05 adopted in "Code for Seismic Design of Highway Bridges" of China (JTG/T B02-01-2008) is determined by

$$S = \begin{cases} S_{\max}(5.5T + 0.45), & T < 0.1\,\text{s}, \\ S_{\max}, & 0.1\,\text{s} \le T < T_g, \\ S_{\max}\left(\dfrac{T_g}{T}\right), & T \ge T_g. \end{cases} \quad (1)$$

T_g indicates the characteristic period of the response spectrum. According to the characteristic periodic zoning map of the acceleration response spectrum of China's earthquake ground motion, $T_g = 0.40$ s. T indicates the natural period of the structure. $S_{\max}$ indicates the maximum value of the horizontal design acceleration response spectrum.

Under the action of the E1 earthquake, the importance coefficient $C_i = 0.5$; site coefficient $C_s = 1.0$; damping adjustment coefficient $C_d = 1.0$; A is the peak value of horizontal design basic ground motion acceleration, and $A = 0.15$ g is selected according to Zoning Map of the Seismic Parameters of China. Therefore, $S_{\max} = 2.25 C_i C_s C_d A = 1.654\ \text{m/s}^2$, which is the horizontal design response adopted in the seismic analysis of the structure.

The design response spectrum curve in the horizontal direction used for seismic analysis of structures is shown in Figure 17.

Tables 1 and 2 show the distribution of the first 10 frequencies of the original bridge is concentrated between 1.741 Hz and 4.408 Hz; the distribution of the first 10 frequencies of the reinforced bridge is concentrated between 2.103 Hz and 9.078 Hz. The results show that the frequency band of the bridge is narrow; that is, the distribution of the vibration mode of the curved truss bridge is relatively dense. In the combination of modes, the spatial coupling should be considered. Therefore, CQC (Complete Quadratic Combination) method is selected to calculate the seismic effect.

Referring "Code for Seismic Design of Highway Bridges" of China, in the first 200 vibration modes of the bridge, the sum of modal participating mass ratios in X, Y, and Z directions of the original bridge is between 92.39% and 96.99%, as shown in Table 3.

The CQC method is used to input the longitudinal, transverse, and vertical seismic effects of the bridge. According to "Rules for Seismic Design of Highway Bridges" of China (JTJ004-89), three directions of seismic action are considered as three working conditions to test the maximum response of the structure in the most unfavorable seismic action direction:

Condition 1: EX + 0.3EY + 0.3EZ.

Condition 2: 0.3EX + EY + 0.3EZ.

Condition 3: 0.3EX + 0.3EY + EZ.

Note. EX is the seismic action along the longitudinal direction of the bridge, EY is the seismic action along the transverse direction of the bridge, and EZ is the seismic action along the vertical direction of the bridge.

4.1. Analysis of the Seismic Response of Bridge before Reinforcement

4.1.1. Analysis of Internal Force. The peak values of internal force at the upper chord of the bridge are shown in Table 4 under different working conditions.

Table 4 shows, under three working conditions, the axial force of the top chord of the bridge is far greater than the shear force and axial force, and the maximum value of the axial force appears at the fixed end of the top chord. In condition 2, the out-of-plane bending moment of each typical section of the bridge increases obviously, which is consistent with the out-of-plane transverse vibration of the main truss in the first mode of the bridge. The results show that the out-of-plane stiffness of the main truss is relatively weak. In addition, the maximum values of shear force and axial force appear at the fixed end of the top chord. Therefore, in the reinforcement and aseismic design of this kind of bridge, we should pay attention to the fixed end of the top chord and the out-of-plane stiffness of the main truss.

4.1.2. Analysis of Displacement. The peak values of displacement at the upper chord of the bridge are shown in Table 5 under different working conditions.

Table 5 shows, under three working conditions, the lateral displacement of the bridge is far greater than the longitudinal and vertical displacement, and the maximum lateral displacement occurs at 1/2L of the bridge. In condition 2, the transverse displacement of each typical cross section of the bridge increases obviously. The results show that the transverse stiffness of the main truss of the bridge is insufficient. In addition, because of the small vertical and torsional stiffness of the bridge deck system, the local vertical bending vibration of the bridge deck system is easy to excite the transverse bending vibration of the web member and the out-of-plane vibration of the web member, which results in the larger transverse vibration and displacement of the whole bridge. Therefore, the out-of-plane vibration of the web member and the transverse stiffness of the main truss should be paid attention to in the reinforcement and seismic design.

4.2. Analysis of the Seismic Response of the Bridges after Reinforcement

4.2.1. Analysis of Internal Force. The peak values of internal force at the upper chord of the bridge are shown in Table 6 under different working conditions.

Table 6 shows, under different working conditions, the axial force of the bridge is the largest, the shear force and the bending moment are small, and the maximum internal force appears at the two ends of the upper chord. The maximum

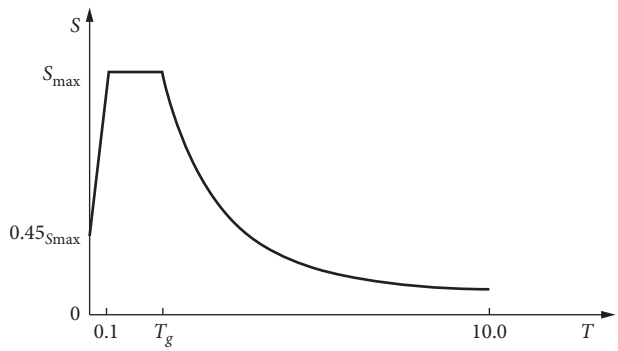

Figure 17: Design response spectrum curve in the horizontal direction.

Table 3: Sum of mass coefficients of mode participation.

Modal number	*X* longitudinal direction (%)	*Y* transverse direction (%)	*Z* vertical direction (%)
200	96.20	92.39	96.99

Table 4: The peak values of the internal force of the bridge.

Working conditions	Typical section	Axial force (kN)	Transverse shear (kN)	Vertical shear (kN)	In-plane bending moment (kN·m)	Out-of-plane bending moment (kN·m)
1	Fixed end	7107.28	26.26	201.04	245.23	179.34
	1/4L	6230.75	23.13	40.63	174.04	69.03
	1/2L	5762.37	14.84	56.11	172.72	56.27
	3/4L	6156.28	22.56	39.26	101.58	70.89
	Active side	6999.42	26.46	189.54	177.13	177.22
2	Fixed end	7040.11	33.53	191.18	202.00	391.85
	1/4L	6142.36	63.16	38.98	144.75	191.30
	1/2L	5711.40	26.16	52.55	168.48	57.83
	3/4L	6120.52	62.12	38.63	94.61	199.75
	Active side	7000.37	33.66	185.68	177.34	391.51
3	Fixed end	7101.63	26.96	192.03	206.22	181.07
	1/4L	6255.10	23.28	39.90	148.91	68.53
	1/2L	5835.26	15.86	53.91	175.35	60.52
	3/4L	6232.60	22.85	39.49	97.73	70.53
	Active side	7067.71	27.08	187.15	181.86	180.56

Table 5: The peak values of displacement of the bridge.

Working conditions	Typical section	UX (mm)	UY (mm)	UZ (mm)	ROTX (rad)	ROTY (rad)	ROTZ (rad)
1	Fixed end	0.00	0.00	0.00	0.00	$1.46E-04$	0.00
	1/4L	0.70	5.07	1.58	$6.73E-04$	$4.60E-05$	$2.97E-04$
	1/2L	0.45	8.96	1.38	$8.55E-04$	$9.30E-05$	$2.00E-06$
	3/4L	0.58	5.09	1.05	$6.59E-04$	$3.50E-05$	$3.14E-04$
	Active side	0.55	0.00	0.00	0.00	$1.22E-04$	0.00
2	Fixed end	0.00	0.00	0.00	0.00	$1.10E-04$	0.00
	1/4L	0.30	15.95	0.91	$2.02E-03$	$2.30E-05$	$4.92E-04$
	1/2L	0.19	27.79	1.17	$2.55E-03$	$3.10E-05$	$2.00E-06$
	3/4L	0.19	15.97	0.80	$2.01E-03$	$1.70E-05$	$4.99E-04$
	Active side	0.29	0.00	0.00	0.00	$9.50E-05$	0.00
3	Fixed end	0.00	0.00	0.00	0.00	$1.26E-04$	0.00
	1/4L	0.42	4.87	1.17	$6.65E-04$	$2.50E-05$	$1.98E-04$
	1/2L	0.24	8.52	1.49	$8.58E-04$	$3.30E-05$	$1.00E-06$
	3/4L	0.22	4.88	0.99	$6.60E-04$	$2.20E-05$	$2.03E-04$
	Active side	0.38	0.00	0.00	0.00	$1.15E-04$	0.00

*UX indicates the displacement in the longitudinal direction of the bridge; UY indicates the displacement in the transverse direction of the bridge; UZ indicates the displacement in the vertical direction of the bridge; ROTX indicates the rotation around the *X*-axis; ROTY indicates the rotation around the *Y*-axis; ROTZ indicates the rotation around the *Z*-axis. The following is the same as here.

Table 6: The peak values of the internal force of the bridge.

Working conditions	Typical section	Axial force (kN)	Transverse shear (kN)	Vertical shear (kN)	In-plane bending moment (kN·m)	Out-of-plane bending moment (kN·m)
1	Fixed end	4977.01	20.31	398.83	778.69	300.28
	1/4L	4329.28	26.18	109.92	433.59	82.61
	1/2L	4037.94	7.77	216.20	406.37	31.00
	3/4L	4331.43	25.85	76.89	398.83	86.92
	Active side	4912.23	20.96	370.48	589.34	303.32
2	Fixed end	4905.89	47.11	378.36	727.27	924.61
	1/4L	4241.07	83.52	113.45	443.74	264.87
	1/2L	3938.51	20.32	223.20	406.23	84.68
	3/4L	4278.33	82.39	77.81	397.34	275.99
	Active side	4882.07	46.91	359.78	587.90	923.19
3	Fixed end	4960.34	20.75	412.73	761.11	301.82
	1/4L	4356.17	25.55	120.27	467.74	81.28
	1/2L	4070.56	7.60	210.64	399.45	30.90
	3/4L	4393.67	25.28	76.97	416.18	84.45
	Active side	4951.64	20.59	385.77	628.42	301.00

Table 7: The peak values of displacement of the bridge.

Working conditions	Typical section	UX (mm)	UY (mm)	UZ (mm)	ROTX (rad)	ROTY (rad)	ROTZ (rad)
1	Fixed end	0.00	0.00	0.00	0.00	$1.09E-04$	0.00
	1/4L	0.53	3.59	1.19	$4.22E-04$	$2.90E-05$	$2.75E-04$
	1/2L	0.35	8.03	1.13	$6.68E-04$	$4.70E-05$	0.00
	3/4L	0.40	3.60	1.12	$4.26E-04$	$2.80E-05$	$2.82E-04$
	Active side	0.48	0.00	0.00	0.00	$9.00E-05$	0.00
2	Fixed end	0.00	0.00	0.00	0.00	$7.40E-05$	0.00
	1/4L	0.31	11.72	0.83	$1.35E-03$	$2.40E-05$	$8.43E-04$
	1/2L	0.18	25.99	0.93	$2.17E-03$	$1.70E-05$	0.00
	3/4L	0.13	11.72	0.80	$1.35E-03$	$2.30E-05$	$8.46E-04$
	Active side	0.31	0.00	0.00	0.00	$5.90E-05$	0.00
3	Fixed end	0.00	0.00	0.00	0.00	$1.15E-04$	0.00
	1/4L	0.62	3.53	1.59	$4.11E-04$	$3.90E-05$	$2.59E-04$
	1/2L	0.33	7.86	1.07	$6.60E-04$	$2.10E-05$	0.00
	3/4L	0.15	3.53	1.41	$4.12E-04$	$3.90E-05$	$2.60E-04$
	Active side	0.54	0.00	0.00	0.00	$9.80E-05$	0.00

axle force of reinforced bridge decreases compared with that before reinforcement.

4.2.2. Analysis of Displacement. The peak values of displacement at the upper chord of the bridge are shown in Table 6 under different working conditions.

Table 7 shows, under various circumstances, the displacement of each critical section of the bridge after reinforcement decreases.

4.3. Comparative Analysis of the Seismic Response of Bridges before and after Reinforcement. To study the effect of reinforcement measures on the seismic behavior of the concrete-filled steel tubular curved truss girder bridge, according to the peak values of internal force and displacement of the bridge at the chord, the responses of bridges are compared and analyzed.

4.3.1. Analysis of Internal Force. In order to analyze the internal force variation of the bridge before and after reinforcement, the internal force peak values at the fixed end of the bridge are extracted, as shown in Table 8, and a comparison diagram of the peak values of the internal force is given here, as shown in Figure 18.

Figure 18 shows, under the same condition, compared with that before reinforcement, the axial force of the bridge after reinforcement is reduced by about 30%. Table 8 shows, under the action of each condition, the upper chord has the largest axial force and the smaller shear force and bending moment. Under the condition of condition 2, the lateral shear force and an out-of-plane bending moment of the bridge increase more obviously than those under the other two conditions. The result shows that the cross-bridge stiffness of the bridge is relatively weak, which is sensitive to the ground motion in the transverse direction of the bridge.

4.3.2. Analysis of Displacement. In order to analyze the displacement of bridges before and after reinforcement, the peak values of the displacement at the position of 1/2L and the mid-span position of the bridge deck are extracted, as shown in Tables 9 and 10. The comparison of the transverse

Table 8: Comparison of peak values of internal force at the fixed end of the bridge before and after reinforcement.

Bridge status	Working conditions	Axial force (kN)	Transverse shear (kN)	Vertical shear (kN)	In-plane bending moment (kN·m)	Out-of-plane bending moment (kN·m)
Before reinforcement	1	7107.28	26.26	201.04	245.23	179.34
	2	7040.11	33.53	191.18	202.00	391.85
	3	7101.63	26.96	192.03	206.22	181.07
After reinforcement	1	4977.01	20.31	398.83	778.69	300.28
	2	4905.89	47.11	378.36	727.27	924.61
	3	4960.34	20.75	412.73	761.11	301.82

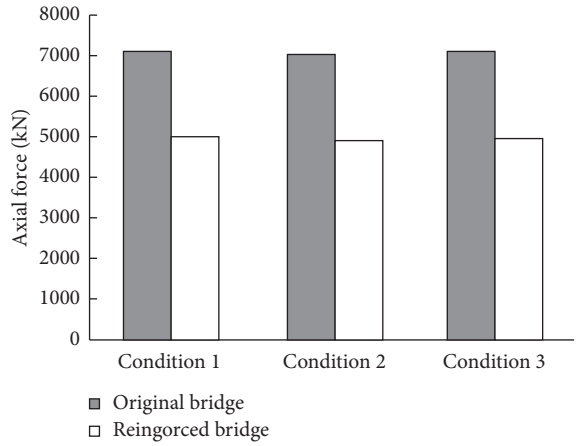

Figure 18: Comparison of peak values of axial force at the fixed end of the bridge before and after reinforcement.

Table 9: Comparison of peak values of displacement at 1/2L of the upper of the bridge before and after reinforcement.

Bridge status	Working conditions	UX (mm)	UY (mm)	UZ (mm)	ROTX (rad)	ROTY (rad)	ROYZ (rad)
Before reinforcement	1	0.45	8.96	1.38	$8.55E-04$	$9.30E-05$	$2.00E-06$
	2	0.19	27.79	1.17	$2.55E-03$	$3.10E-05$	$2.00E-06$
	3	0.24	8.52	1.49	$8.58E-04$	$3.30E-05$	$1.00E-06$
After reinforcement	1	0.35	8.03	1.13	$6.68E-04$	$4.70E-05$	0.00
	2	0.18	25.99	0.93	$2.17E-03$	$1.70E-05$	0.00
	3	0.33	7.86	1.07	$6.60E-04$	$2.10E-05$	0.00

Table 10: Comparison of peak values of displacement at the mid-span position of bridge decks before and after reinforcement.

Bridge status	Working conditions	UX (mm)	UY (mm)	UZ (mm)
Before reinforcement	1	0.611	0.247	5.825
	2	0.320	0.710	6.389
	3	0.723	0.285	16.397
After reinforcement	1	0.460	0.181	2.265
	2	0.253	0.542	2.007
	3	0.523	0.196	3.946

displacement at the position of 1/2L of the upper chord of the bridge and the vertical displacement at the mid-span of the bridge deck before and after reinforcement is given, as shown in Figures 19 and 20.

Tables 9 and 10 and Figures 19 and 20 show, under the three conditions, compared with that before reinforcement, the transverse displacement at the position of 1/2L of the bridge after reinforcement decreases by 10.4%, 6.5%, and 7.7%, respectively. The vertical displacement of the bridge is reduced by 18.1%, 28.6%, and 20.0%, respectively. The vertical displacement of the bridge deck at mid-span decreases by 61.1%, 68.6%, and 75.9%, respectively. It shows that the reinforcement measures have improved the lateral stiffness of the bridge and the vertical stiffness of the bridge. Notably, the stiffness of the bridge deck system is improved remarkably.

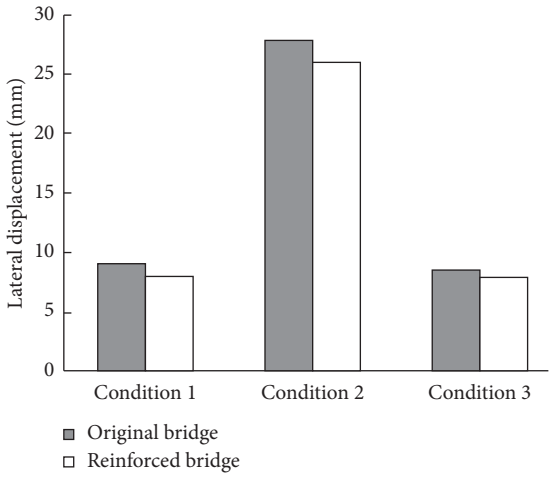

Figure 19: Comparison of peak values of displacement at 1/2L of the upper chord of the bridge before and after reinforcement.

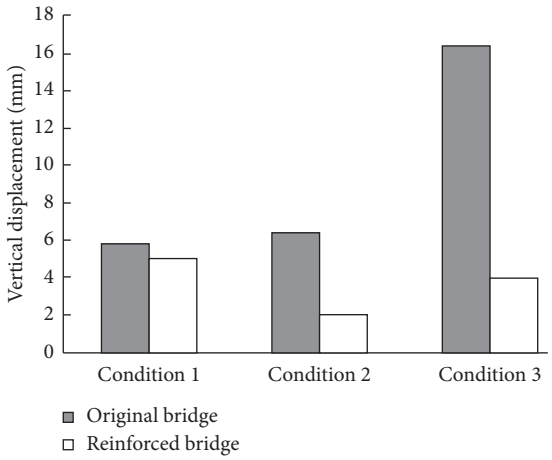

Figure 20: Comparison of peak values of displacement at the mid-span position of bridge deck before and after reinforcement.

5. Conclusions

The spatial finite element model of the concrete-filled steel tubular curved truss girder bridge before and after reinforcement was established by using the general finite element software ANSYS, according to its reinforcement scheme. Then, the natural frequencies of the bridge before and after reinforcement were calculated. Finally, the seismic performance of the bridge was analyzed by using the response spectrum method. After comparing and analyzing the calculated results, the following conclusions are drawn:

(1) Both before and after the reinforcement, the first vibration mode of the bridge was the transverse vibration of the main truss, which indicates that the transverse rigidity of the main truss was relatively low. The frequency value of the bridge after reinforcement has increased to varying degrees; in particular, the vertical and torsional frequencies of the bridge increase significantly.

(2) Under different working conditions, the axial force of the upper chord force of the bridge before and after reinforcement is the largest, the shearing force and bending moment are small, and the maximum internal force appears at the two ends of the upper chord. This position should be taken as a weak link in the earthquake resistance of bridges. Under the same conditions, the axial force of the bridge after reinforcement is reduced by about 30% compared with that before reinforcement.

(3) Under different working conditions, the transverse displacement is larger than the longitudinal and vertical displacement, and the angular displacement is relatively small. The displacement of the bridge after reinforcement decreases in varying degrees compared with that before reinforcement. The reinforcement measures improve the lateral stiffness of the bridge, and the vertical stiffness of the bridge is improved; in particular, the stiffness of the bridge deck is improved significantly.

Data Availability

The data are available in this manuscript. The data in this manuscript were obtained through a series of calculations and analyses. The related data used to support the findings of this study are available from the corresponding author upon request.

Conflicts of Interest

The authors confirm that there are no conflicts of interest in this paper.

Acknowledgments

The authors thank the National Nature Science Foundation of China (grant number 51408557), the Henan Provincial Transportation Technology Project (2020J-2-6), and China Postdoctoral Science Foundation (grant number 2013M541995) for their support.

References

[1] B. Sevim, S. Atamturktur, A. C. Altunişik, and A. Bayraktar, "Ambient vibration testing and seismic behavior of historical arch bridges under near and far fault ground motions," *Bulletin of Earthquake Engineering*, vol. 14, no. 1, pp. 241–259, 2016.

[2] E. M. Farahani and S. Maalek, "An investigation of the seismic behavior of a deck-type reinforced concrete arch bridge," *Earthquake Engineering and Engineering Vibration*, vol. 16, no. 3, pp. 609–625, 2017.

[3] P. Zampieri, G. Tecchio, F. Da Porto, and C. Modena, "Limit analysis of transverse seismic capacity of multi-span masonry arch bridges," *Bulletin of Earthquake Engineering*, vol. 13, no. 5, pp. 1557–1579, 2015.

[4] P. Zampieri, M. A. Zanini, and C. Modena, "Simplified seismic assessment of multi-span masonry arch bridges," *Bulletin of Earthquake Engineering*, vol. 13, no. 9, pp. 2629–2646, 2015.

[5] C. Shao, J.-w. W. Ju, G. Han, and Y. Qian, "Seismic applicability of a long-span railway concrete upper-deck arch bridge with CFST rigid skeleton rib," *Structural Engineering and Mechanics*, vol. 11, no. 5, pp. 645–655, 2017.

[6] F. d. Porto, G. Tecchio, P. Zampieri, C. Modena, and A. Prota, "Simplified seismic assessment of railway masonry arch bridges by limit analysis," *Structure and Infrastructure Engineering*, vol. 12, no. 5, pp. 567–591, 2015.

[7] K. Deng, G. Yan, H. Yang, and C. Zhao, "RC arch bridge seismic performance evaluation by sectional N-M interaction and coupling effect of brace beams," *Engineering Structures*, vol. 183, no. 5, pp. 18–29, 2019.

[8] R. Li, X. Yuan, W. Yuan, X. Dang, and G. Shen, "Seismic analysis of half-through steel truss arch bridge considering superstructure," *Structural Engineering and Mechanics*, vol. 59, no. 3, pp. 387–401, 2016.

[9] G. Xiao, X. Kaizhong, B. Meiyan et al., "Influence of Karst cave on seismic response analysis of concrete filled steel tubular arch bridge," *Highway*, vol. 6, pp. 172–176, 2018.

[10] O. Yangjing, L. Jianmao, L. Shangshun et al., "Seismic design of concrete-filled steel tubular lattice high-rise continuous beam bridge," *Journal of Chongqing University*, vol. 41, no. 9, pp. 94–104, 2018, in Chinese.

[11] F.-y. Huang, C. Fu, Y.-z. Zhuang, and Z.-h. Xiong, "Experiment on seismic performance of concrete filled steel tubular arch-rib under multi-shaking-tables," *Thin-Walled Structures*, vol. 116, pp. 212–224, 2017.

[12] L.-H. Han, W. Xu, S.-H. He, and Z. Tao, "Flexural behaviour of concrete filled steel tubular (CFST) chord to hollow tubular brace truss: experiments," *Journal of Constructional Steel Research*, vol. 109, pp. 137–151, 2015.

[13] Z. Bo, L. Shucai, Y. Xueying et al., "Seismic response analysis of long-span CFST arch bridges with upper support," *Journal of Highway and Transportation Research and Development*, vol. 26, no. 3, pp. 65–73, 2009, in Chinese.

[14] Z. Shixiong, Z. Shuhua, and W. Dongsheng, "Seismic response performance of long span CFST arch bridges," *Journal of Southwest Jiaotong University*, vol. 34, no. 3, pp. 320–324, 1999, in Chinese.

[15] J. J. Álvarez, A. C. Aparicio, J. M. Jara, and M. Jara, "Seismic assessment of a long-span arch bridge considering the variation in axial forces induced by earthquakes," *Engineering Structures*, vol. 34, pp. 69–80, 2012.

[16] D. Xiaobing and C. Yijuan, "Seismic response analysis of five-span concrete filled steel tubular arch bridge," *Highway*, vol. 2, pp. 98–102, 2016.

[17] H. Zhiming, L. Jingying, and H. Tianyi, "Seismic response analysis of concrete filled steel tubular arch bridge based on traveling wave effect," *Bridge Construction*, vol. 1, pp. 25–28, 2010.

[18] X. Yan and H. Shide, "Dynamic stability of concrete filled steel tubular arch bridge under earthquake," *Journal of Tongji University (Natural Science)*, vol. 03, pp. 315–319, 2007, in Chinese.

[19] L.-x. Wang, Q.-y. Liu, S.-k. Di, and C.-s. Xiang, "Analysis of stationary random seismic response of arch bridge with concrete-filled steel tubes under non-uniform excitation," *Journal of Lanzhou University of Technology*, vol. 42, no. 2, pp. 124–129, 2016, in Chinese.

[20] H. Yuan, J. Dang, and T. Aoki, "Behavior of partially concrete-filled steel tube bridge piers under bi-directional seismic excitations," *Journal of Constructional Steel Research*, vol. 93, pp. 44–54, 2014.

[21] Y.-F. Yang, M. Liu, C. Hou, and X.-M. Bie, "Behaviour of four-legged square CFST latticed members under lateral cyclic loading," *Journal of Constructional Steel Research*, vol. 156, pp. 54–74, 2019.

[22] Y.-F. Yang, C. Hou, Z. Wen, and L.-H. Han, "Experimental behaviour of square CFST under local bearing forces," *Thin-Walled Structures*, vol. 74, pp. 166–183, 2014.

[23] L. Xiaozhen, Y. Dehai, L. Kangning et al., "Seismic response of continuous beam-arch bridge under spatially varying ground motions," *Journal of Southwest Jiaotong University*, vol. 1, pp. 1–9, 2020, in Chinese.

[24] R. Yadav, H. Yuan, B. Chen, and Z. Lian, "Experimental study on seismic performance of latticed CFST-RC column connected with RC web," *Thin-Walled Structures*, vol. 126, pp. 258–265, 2018.

[25] Y. Di, L. He, and Z. Sumei, "Elastic-plastic time-history analysis of half-through CFST bridge," *Journal of Jilin University (Engineering and Technology Edition)*, vol. 44, no. 6, pp. 1633–1638, 2014, in Chinese.

[26] G. Jianxin, X. Wei, X. Lijun et al., "Research on reinforcement technique to enhance lateral stiffness of steel truss bridge on existing railway," *China Railway Science*, vol. 5, pp. 12–16, 2005, in Chinese.

[27] S. Chen, C. Hou, H. Zhang, and L.-H. Han, "Structural behaviour and reliability of CFST trusses with random initial imperfections," *Thin-Walled Structures*, vol. 143, Article ID 106192, 2019.

[28] P. Kai, Q. Fenyi, and J. Xiaofei, "Strengthening technique of prestressing hinged piecewise steel arches for arch bridges," *Journal of Chongqing Jiaotong University (Natural Science)*, vol. 36, no. 4, pp. 12–17, 2017, in Chinese.

[29] D.-Y. Ma, L.-H. Han, and X. L. Zhao, "Seismic performance of the concrete-encased CFST column to RC beam joint: experiment," *Journal of Constructional Steel Research*, vol. 154, pp. 134–148, 2019.

[30] C. Baochun, L. Fuzhong, and W. Jiangang, "Statistical analysis on 327 CFST arch bridges," *Journal of China & Foreign Highway*, vol. 31, no. 3, pp. 96–103, 2011, in Chinese.

[31] D. Chen, W. Wang, Z. Li, Z. Xu, and F. Ma, "Comparative analysis of seismic performance of 122-meter long concrete-filled steel tube arched chord truss bridge before and after reinforcement," *Journal of Asian Architecture and Building Engineering*, vol. 19, no. 2, pp. 90–102, 2020.

[32] R. Xin, S. Xuefei, B. Guiping et al., "Risk analysis of class II stability of Taipinghu bridge," *Bridge Construction*, vol. 5, pp. 24–27, 2006.